

Variable characteristics of the wintertime net heat flux along the Kuroshio system and its association with climate in China

Shanshan Wang,^{a,b} Yuping Guan,^{b*} Zhijian Li,^c Yi Chao^c and Jianping Huang^a

^a Key Laboratory for Semi-Arid Climate Change of the Ministry of Education, College of Atmospheric Sciences, Lanzhou University, China

^b State Key Laboratory of Tropical Oceanography, Chinese Academy of Sciences, South China Sea Institute of Oceanology, Guangzhou, China

^c Joint Institute for Regional Earth System Science and Engineering, University of California, Los Angeles, CA, USA

ABSTRACT: On the basis of the datasets obtained for the monthly turbulent heat flux (1984–2009) from the Objectively Analyzed Air–Sea Heat Flux (OAFlux), the radiation flux from the International Satellite Cloud Climatology Project (ISCCP), the variability characteristics of the net heat flux (Qnet) over the Kuroshio System (KS) and its relationship with the climate in China were studied. The results reveal that except for a steady enhancement in the period 1984–2009, the boreal winter Qnet over the KS is characterized by obvious interannual variation of the period quasi-5 year as well as decadal variability shifting from negative to positive anomalies in the mid-1990s. In the wintertime, the increasing KS Qnet is primarily responsible for the intensification of the East Asia winter monsoon (EAWM) via a deepening of the Aleutian low and an enhancement of the Siberia high and has a correlation coefficient of 0.72 with a 1-month delay. The enhanced-EAWM induces colder winters in Northeast China and higher Qnet over the KS by carrying significantly greater amounts of cold air mass. During the low Qnet winter, the EAWM is weakened, and the southwesterly wind that contains abundant water vapour enhances and pushes toward southern China, thereby bringing heavier rainfall. The anomalous Qnet over the KS in the wintertime lasts until the following spring with a weaker relative intensity. In the spring after the low KS Qnet winter, the anomalous easterly wind transfers colder air masses from the Sea of Japan to the North China and Yellow–Huaihe regions and then cools these regions. The warmer and wetter southwesterlies along the northwestern flank of the anomalous anticyclone east of Taiwan Island meet these colder easterlies accompanied by an anomalous upward motion, thereby inducing an anomalous northwest–southeast precipitation band in the central and eastern region of China, especially in the Yangtze–Huaihe region.

KEY WORDS Kuroshio system; net heat flux; temperature; precipitation; China

Received 16 August 2013; Revised 12 April 2014; Accepted 28 April 2014

1. Introduction

The Kuroshio System (KS) comprises the Kuroshio current and Kuroshio extension (KE) and is one of the strong western boundary currents in the North Pacific. It transports enormous volumes of warm saline water from the tropics to the mid-latitudes, thereby redistributing differential heat accumulated from solar radiation fluxes and influencing the overlying circulation (e.g. Wallace and Gutzler, 1981; Tomita *et al.*, 2007; Kelly *et al.*, 2010; Kwon *et al.*, 2010). China is located west of the KS, and its climate may be influenced via the atmospheric responses to the variations of the KS variables, such as path, transport velocity, sea surface temperature (SST), and heat fluxes. Joyce *et al.* (2009) suggested that the shift in the latitudes of the KE path can cause substantial changes in SST, which may influence synoptic atmospheric variability with little delay. Tokinaga *et al.* (2006) revealed that SST gradients over the KE induce strong

wind convergences and then cause local cloud thickening. Wang *et al.* (1980) indicated that the KS activity is closely related to East Asia atmospheric circulation patterns with an enhanced East Asia Trough circulation during negative SST anomalies over the KS region. These anomalous SST patterns over the KS may result in precipitation anomalies in different regions of China, e.g. the Yangtze River region, North China, and the Huang-huai Plain (e.g. Weng *et al.*, 1996; Zhang *et al.*, 1999; Li and Ding, 2002; Ni *et al.*, 2004), and also impact the air temperature in China (Zhao *et al.*, 2007).

The atmosphere interacts with the ocean through air–sea fluxes, not SST, although SST is a key variable that affects air–sea heat exchange processes (Yu and Weller, 2007). Relative to the SST, the heat flux variations, especially the total net heat flux (Qnet), at the air–sea interface contain richer information. The air and sea exchange heat at their interface via a number of processes, including solar radiation (SW), longwave radiation (LW), sensible heat flux (SHF) by conduction and convection, and latent heat flux (LHF) by evaporation of sea surface water (Yu and Weller, 2007). The turbulent flux (sum of the SHF and LHF) is the major cause of ocean heat loss in the variability of sea–air

*Correspondence to: Y. Guan, State Key Laboratory of Tropical Oceanography, Chinese Academy of Sciences, South China Sea Institute of Oceanology, Guangzhou 510301, China. E-mail: guan@scsio.ac.cn

exchanges in the boreal winter followed by radiative cooling because of net outgoing LW; the SW is small, but it is the major contributor to the heat gain in oceans in winter. Recently, a paper in *Nature* by Gulev *et al.* (2013) argued for the importance of surface turbulent fluxes in the Atlantic and stated that it would be important to extend the analysis to the radiative components of air–sea exchanges to complete the surface heat balance, which is crucial as a driving factor (Booth *et al.*, 2012). Therefore, this study emphasizes the Qnet variation along the KS region and its climate effect in China. Previous studies have indicated that the heat flux variations over the KS have the potential to influence the atmospheric circulation via variations in storm tracks (Chang *et al.*, 2002; Hoskins and Hodges, 2002; Nakamura *et al.*, 2004; Bengtsson *et al.*, 2006). In their 1990 publication, Hoskins and Valdes (1990) demonstrated that the heat flux over the KS develops a cyclonic cumulus convection, thereby promoting the organization of a precipitation band (see also Minobe *et al.*, 2008). Zhou *et al.* (2011) investigated the influence of the winter turbulent heat flux over the East China Sea, a part of the KS, on the climate in China. Kwon *et al.* (2010) indicated in a review of available studies (e.g. Chang *et al.*, 2002; Nakamura *et al.*, 2004; Wu *et al.*, 2005; Bengtsson *et al.*, 2006; Tokinaga *et al.*, 2009) that the variations of surface heat and moisture fluxes originate mainly from anomalous ocean processes and in turn dampen SST variations and drive the overlying atmospheric circulation, including storm tracks. Liu *et al.* (2006) implied that the Qnet anomalies over the KS east of Taiwan Island warm the overlying atmosphere and promote a low-pressure anomaly at 500 hPa over the North Pacific by the Flexible Global Climate Model. Although substantial studies have been conducted on the relationship between the KS heat fluxes and atmospheric circulation processes, the mechanisms linking the characteristics of the KS to atmospheric circulation are still unclear, in part because of the confounding effects of the Pacific-North America (PNA)-like remote response to interannual variations of the El Niño-Southern Oscillation (ENSO) (Huang *et al.*, 1998; Kelly *et al.*, 2010; Kwon *et al.*, 2010). Therefore, it is required to research the KS variation and its corresponding atmospheric response in detail based on Qnet, which is a direct and comprehensive indicator of the ocean–atmosphere heat exchanges. The first goal of this study is to investigate the Qnet variation feature over the KS region in boreal winter for the period 1984–2009, and the second goal is to explore its impact on the climate in China and its possible process. Conducting such a study is critical and meaningful to deepen the understanding of the mechanisms of air–sea interactions over the KS and might improve regional climate predictions in China.

The datasets and methods used in this study are described in Section 2. Section 3 presents the characteristics of the winter Qnet over the KS (Section 3.1.) and its correlation with the climate in China in the winter (Section 3.2.) and in the following spring (Section 3.3.). Discussion is given in Section 4 followed by the conclusion in Section 5.

2. Data and method

The $1^\circ \times 1^\circ$ heat fluxes between oceans and the atmosphere consist of SW, LW, LH, and SH (Kubota *et al.*, 2002). Qnet is computed as $Q_{net} = SW - LW - LH - SH$. Here, the turbulent heat fluxes have been derived from the Objectively Analyzed Air–Sea Heat Flux (OAFlux) project at the Woods Hole Oceanographic Institution (WHOI) by combining satellite observations with *in-situ* measurements and the outputs of surface meteorological fields from numerical weather prediction (NWP) reanalysis models (Yu and Weller, 2007; Yu *et al.*, 2008). To compute the Qnet, surface SW, and LW were obtained from the International Satellite Cloud Climatology Project (ISCCP; Zhang *et al.*, 2004). The two datasets (OAFlux + ISCCP) are part of the most recent global heat flux products, and their derived Qnet provides the best comparison at measurement sites and is most physically representative among the four products [OAFlux + ISCCP, 40-year Re-Analysis (ERA-40), the National Centers for Environmental Prediction reanalysis-1 (NCEP1) and reanalysis-2 (NCEP2)] (Yu *et al.*, 2007). The monthly surface turbulent heat fluxes are from January 1958 to December 2011, whereas the monthly surface radiation is from July 1983 to December 2009. Thus, this study is based on the monthly mean datasets for the overlapping period of 1984–2009. Note that the signs of the Qnet will be deliberately reversed and the positive values will indicate the heat losses from the ocean to the atmosphere in this study. The monthly mean datasets of temperature, geopotential height, sea level pressure (SLP), wind velocity, and specific humidity were obtained from the National Center for Environmental Protection/National Center for Atmospheric Research (NCEP/NCAR) (Kalnay *et al.*, 1996). We also used the monthly mean surface air temperature (SAT) and precipitation of the 160 stations in China provided by the China Meteorological Administration.

In this study, we mainly applied the empirical orthogonal function (EOF), singular spectrum analysis (SSA), wavelet analysis, and composite analysis. Among them, the SSA was developed to reconstruct the geophysical time series and was mathematically similar to the EOF. It can extract as much reliable information as possible from a short and chaotic time series without inputs of the physical characteristics of the system and can then separate the low-frequency from the high-frequency (Vautard *et al.*, 1992).

3. Results

The KS Qnet has obvious seasonal variation (e.g. Kubota *et al.*, 2002; Wallace and Hobbs, 2006; Bond and Cronin, 2008; Kwon *et al.*, 2010) that is strongest in winter and is dominated mainly by latent heat fluxes because of episodic outbreaks of cold dry air of continental origin (Xue *et al.*, 1995; Ninomiya, 2006; Konda *et al.*, 2010). Therefore, this study focuses on the Qnet variations over the KS during the wintertime (defined here as November–February) during which the oceans lose large amounts of heat to the

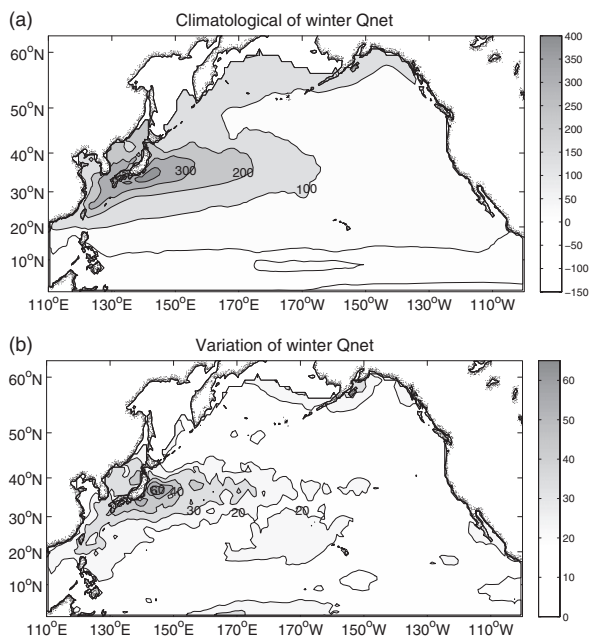


Figure 1. Distribution of (a) the climatological winter Qnet and (b) its variation in the North Pacific based on the period of 1984–2009. Contour intervals (CIs) are 100 W m^{-2} in (a) and 10 W m^{-2} in (b).

overlying atmosphere, which accounts for approximately 65% of the total air–ocean heat exchanges.

3.1. The low-frequency trend and interannual variability of the Qnet intensity

Figure 1 shows the climatological winter mean Qnet distribution in the North Pacific, which indicates that the largest upward Qnet is located around the KS, as revealed by numerous studies (e.g. Cayan, 1992; Frankignoul and Kestenare, 2002; Wallace and Hobbs, 2006). Many indices describe the KS Qnet by averaging the Qnet over a certain rectangular-shaped area, which is not particularly optimum because the select region might not be the most representative for the KS. Therefore, we applied the EOF analysis (North *et al.*, 1982a) to obtain the dominant mode of the KS Qnet. The area we selected extends from 110°E to 180° and 20°N to 55°N . As shown in Figure 1(b), the variance of the Qnet is large over the KS and gradually becomes smaller over its surrounding area; therefore, the data field is normalized in the EOF analysis to avoid the possible influence of inhomogeneous variance on the results in our target area.

Figure 2(a) represents the spatial distribution of the first eigenvector of the normalized Qnet for the period 1984–2009, which accounts for 53% of the total variance and is well separated from the other eigenvalues as per the criterion of North *et al.* (1982b). It is significant that the centre of this mode is located east of the Japan Islands, which is close to the area used in previous studies for defining the intensity indices of the KS. The corresponding principal component (PC) time series with a steady increasing trend is shown in Figure 2(b) (the solid black line). Moreover, we also averaged the Qnet over the region enclosed by the 300 W m^{-2} contour of the

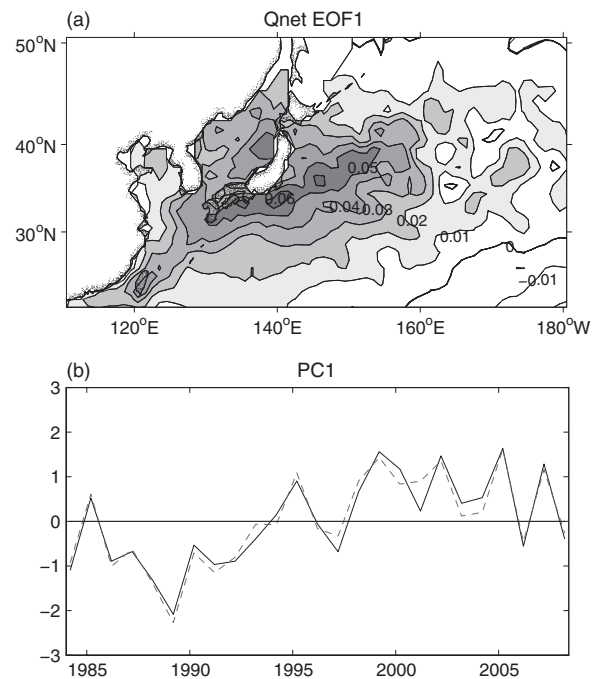


Figure 2. (a) The first EOF mode of the winter mean Qnet for the years 1984–2009. (b) The corresponding normalized PC time series for the first EOF mode (the solid line) and the normalized area-averaged Qnet (the dashed line) with the correlation coefficient of 0.98. The variance explained is 52.6%.

climatological winter mean Qnet (Figure 1(a)) to describe the KS Qnet intensity (Figure 2(b), the red dashed line). The above selected area covers the whole KS and is more representative than a description of the region as a simple rectangular-shape, as has been used in previous studies (Li *et al.*, 2011; Zhou *et al.*, 2011). Note that the derived PC1 and the area-averaged Qnet in Figure 2(b) are both normalized for ease of comparison. The correlation coefficient between the PC1 and the area-averaged Qnet intensity index is 0.98, which is far above the 99% confidence level based on Student's *t*-test. Therefore, the leading EOF of the Qnet over the region (110°E – 180° , 20°N – 55°N) provides an accurate depiction of the variation of the KS Qnet intensity. Using the same analysis on the turbulent heat flux, which is the major contributor to the Qnet, its first EOF pattern (not shown) is highly similar to the Qnet, and their corresponding normalized time series almost overlap with the correlation coefficient of 0.96.

Figure 3 shows the reconstructions of the winter Qnet intensity time series over the KS by applying a SSA. In terms of the reconstructed Qnet time series, the first time principle component (T-PC1) explains 48% of the total variance depicting the low-frequency trend (Figure 3(b), red line). The linear trend of the normalized Qnet PC1 (Figure 3(b), dashed line) is significantly ascending and greater than the 99% confidence level based on Student's *t*-test. Moreover, it is estimated that the averaged Qnet over the region enclosed by the 300 W m^{-2} of the climatological winter increases by 2.6 W m^{-2} per year. The evident ascending trend of the Qnet over the KS from 1984 to 2009 is consistent with previous findings (Zhang *et al.*,

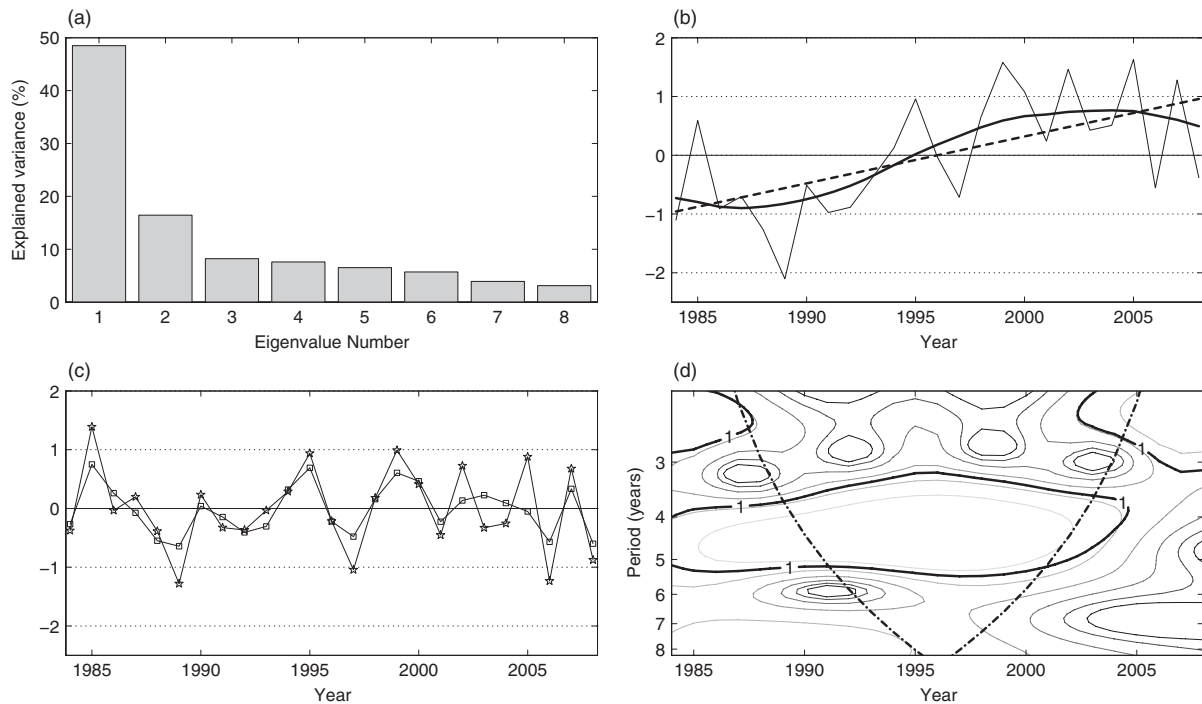


Figure 3. (a) Explained variance of the first eight modes based on SSA. (b) SSA reconstructed low-frequency trend (T-PC1, thick solid line) of the original PC1 time series (thin solid line) plus a linear trend (dashed line). (c) The residual time series of PC1 (solid line with star markers); the reconstructed time series of PC1 based on the sum of T-PC2 to T-PC4 (solid line with square markers) and (d) its corresponding wavelet power spectrum by Wavelet Analysis (thick solid contours represent the 95% confidence level based on Student's *t*-test).

2010; Li *et al.*, 2011; Zhou *et al.*, 2011). In addition, the low-frequency temporal changes appear to show a sine curve-like variability during the period 1984–2009 with a decadal weakening around the mid-1980s, then recovering from negative to positive anomalies around the mid-1990s. The SSA residual time series, which is computed as the difference of the raw time series and reconstructed low-frequency time series, mainly denotes interannual variations of the KS Qnet (Figure 3(c), solid line with star markers). The cumulative explained variance of T-PC2, T-PC3, and T-PC4 (denoted as T-PC2-4 hereafter) is up to 32% (Figure 3(c), solid line with square markers). A wavelet analysis on the T-PC2-4 is shown in Figure 3(d), and most of the power is concentrated in periodicities of 4–5 years throughout the study period. Therefore, the winter KS Qnet not only has an increasing trend but is also characterized by the interannual variations in the period of quasi-5 year as well as the decadal variability. How the atmospheric circulation responds to the above Qnet variability over the KS and what impacts on the climate in China responds to these atmospheric changes will be explored in Sections 3.2. and 3.3., respectively.

3.2. Simultaneous relationship of the winter KS Qnet variation and China climate

Kwon *et al.* (2010), in a review of available studies (e.g. Qiu, 2000; Chang *et al.*, 2002; Nakamura *et al.*, 2004; Bengtsson *et al.*, 2006; Tokinaga *et al.*, 2006), revealed that the variation of surface heat and moisture fluxes are dominated mainly by anomalous ocean processes

and in turn dampen SST variations and drive overlying atmospheric circulation, including storm tracks (e.g. Bond and Cronin, 2008; Joyce *et al.*, 2009; Kwon *et al.*, 2010), thereby influencing the regional climate in East Asia. Along with the obvious interannual and decadal variabilities of the winter KS Qnet for the period 1984–2009, we are interested in the atmospheric response to these air–sea exchange changes and the corresponding climate anomalies in China.

To explore the possible relationship of the regional climate in China and the winter KS Qnet variations, we performed a composite analysis on the normalized PC1 time series as a KS Qnet intensity index. The high and low index cases selected are the winters in which the absolute normalized values of the PC1 are larger than 0.5. On the basis of this criterion, the nine selected high index winters are 1985, 1995, 1998, 1999, 2000, 2002, 2004, 2005, and 2007, and the ten low index winters are 1984, 1986, 1987, 1988, 1989, 1990, 1991, 1992, 1997, and 2006. The remaining 6 years belong to the normal winters.

Figure 4(a) shows the composite difference of the SLP between the low and normal KS Qnet winters. There is a strong high pressure anomaly covering from eastern China to the whole western Northern Pacific, with a northwest-southeast centre around the KS region (30°N–50°N, 120°E–180). West and northeast to this high pressure anomaly, there are two weak low anomalies over Central Asia and the Aleutian region, respectively. A similar structure is shown in the geopotential height at 500 hPa with a larger negative area in Asia, as indicated in Figure 4(b). There is also a southwest–northeast

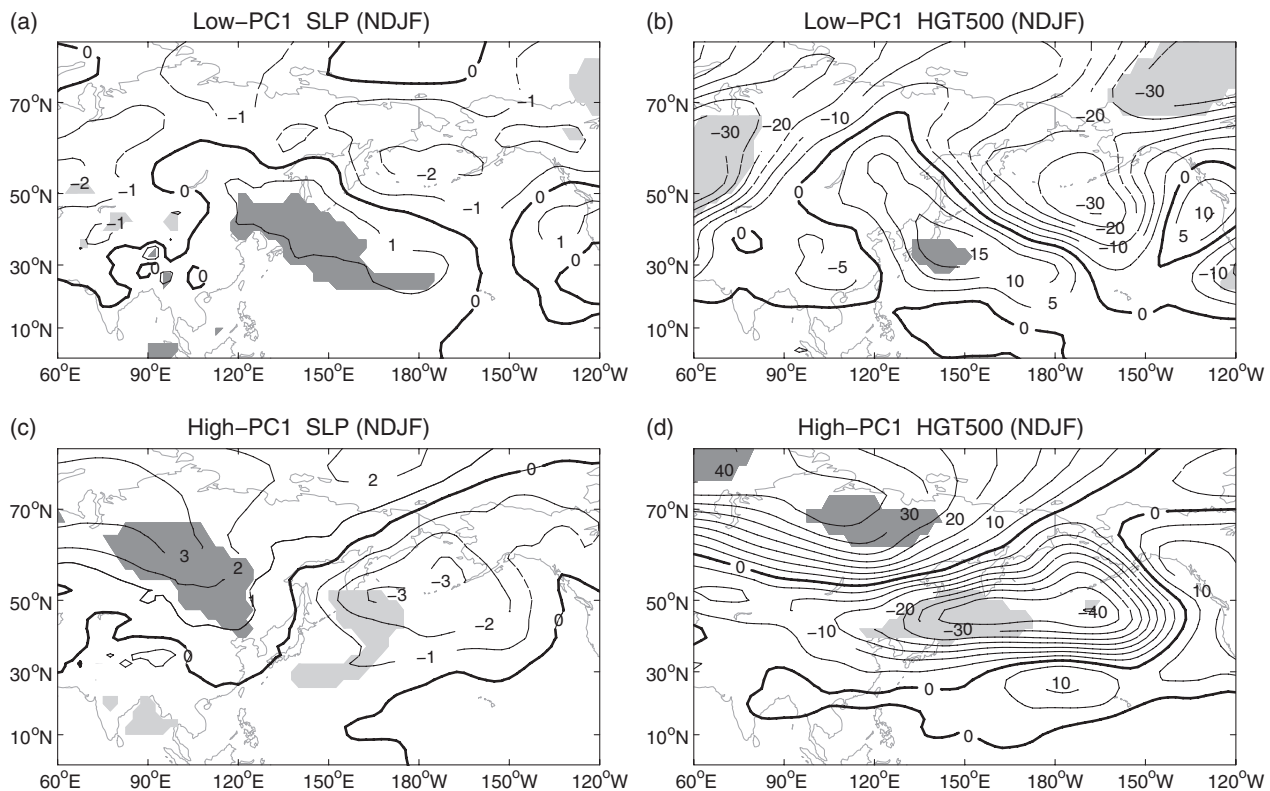


Figure 4. Composite differences of (left) SLP (CI = 1 hPa) and (right) 500 hPa geopotential height (CI = 5 gpm) between (upper) the low and normal KS Qnet winters and (below) the high and normal KS Qnet winters. The shading indicates the 95% confidence level based on Student's *t*-test.

dipole structure in the subtropical North Pacific with an anomalous high pressure centre around the KS and a reverse centre over the Aleutian region. Correspondingly, Figure 4(c) and (d) show the composite difference of the SLP and geopotential height at 500 hPa between the high and normal KS Qnet winters. In contrast, there is a significantly negative centre of SLP over the western and central North Pacific and a strong positive centre around Lake Baikal for high KS Qnet winters. This northwest-southeast dipole is more obvious at 500 hPa, covering the whole subtropical North Pacific and Siberia, and corresponds to a deepening Aleutian low and an enhancing Siberia high. Figure 5 presents the composites for the zonal winds in the upper troposphere (300 hPa) and vapour transportation in the lower troposphere (850 hPa) for low and high KS Qnet winters. During the low KS Qnet winters, there is an anomalously negative band extending from eastern China to southern Japan (Figure 5(a)), implying that the East Asian subtropical westerly jet is weakening. In the low-level troposphere, the cold and dry northwesterly is weaker, at the same time, an anomalous anti-cyclone exists over the South China Sea (figure of wind at 850 hPa is not shown) that transfers large amounts of water vapour to southern China, thereby inducing abnormal convergence over these regions (Figure 5(b)) (Wang and Feng, 2011). While the Qnet is in the high phase, an anomalous westerly band appears between 30°N and 50°N with a centre ranging from east Japan to the central Pacific, indicating that the subtropical westerly jet is accelerating (Figure 5(c)). Contrary to Figure 5(b), a significant anomalous cyclone

for the low-level water vapour transportation occurs during the high Qnet winters but is confined in the South China Sea. Then the anomalous water vapour from the westerly and easterly flow converges mostly occur in the sea and only a small part over the coastal zone of southern China (Figure 5(d)).

Figure 6 shows the corresponding composites for air temperature and its advection at 850 hPa in low and high KS Qnet winters. As indicated in Figure 6(a), the air temperature change is small and insignificant, which indicates that the low Qnet over the KS has little influence on the winter temperature in China. It should be noted that variations of air temperature cannot be fully explained by temperature advection during the low Qnet winters, because the corresponding cold advection over the Inner Mongolia province, however, is slightly damped, and the warm advection enhances over southern China because of the anomalous warm advection (warm shading in Figure 6(b)). The anomalous air temperature at 850 hPa in the high KS Qnet winters shows significant cooling from Northeast China across northern Japan to the central North Pacific (Figure 6(c)). There also exists an anomalously negative temperature advection at 850 hPa east of Lake Baikal with the centre around the Japan Islands and KS, meaning that the cold advection is enhanced in these regions (Figure 6(d)). The composite map of station-based SAT in China between the high and low phase of the KS Qnet confirms that the winter is colder in Northern China during the high phase of the KS Qnet (Figure 7(a)) with respect to its low phase.

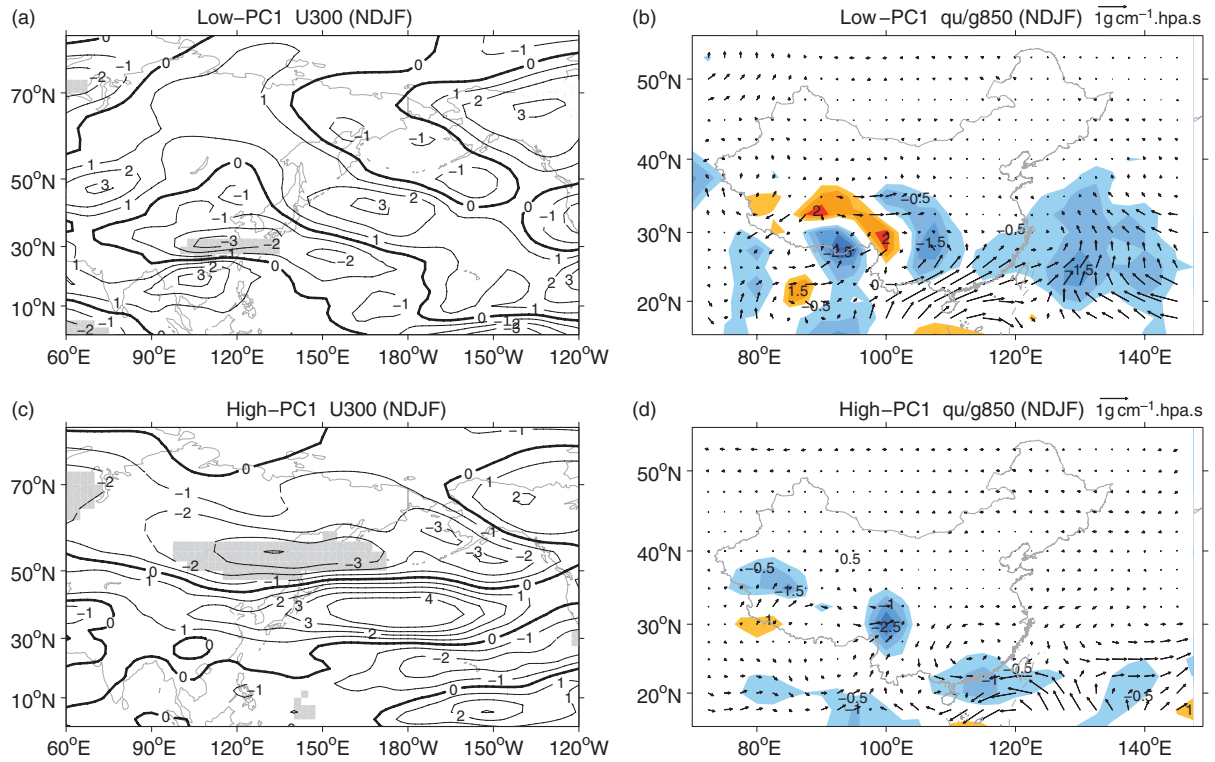


Figure 5. Composite differences of (left) 300 hPa zonal winds ($CI = 1 \text{ m s}^{-1}$) and (right) 850 hPa vapour flux (vector, $\text{g cm}^{-1} \cdot \text{hpa} \cdot \text{s}$) and the corresponding divergence (colour shading, $10^{-8} \text{ g cm}^{-2} \cdot \text{hpa} \cdot \text{s}$) between (upper) the low and normal KS Qnet winters and (below) the high and normal KS Qnet winters. The grey shading in the left panels indicates the 95% confidence level based on Student's *t*-test.

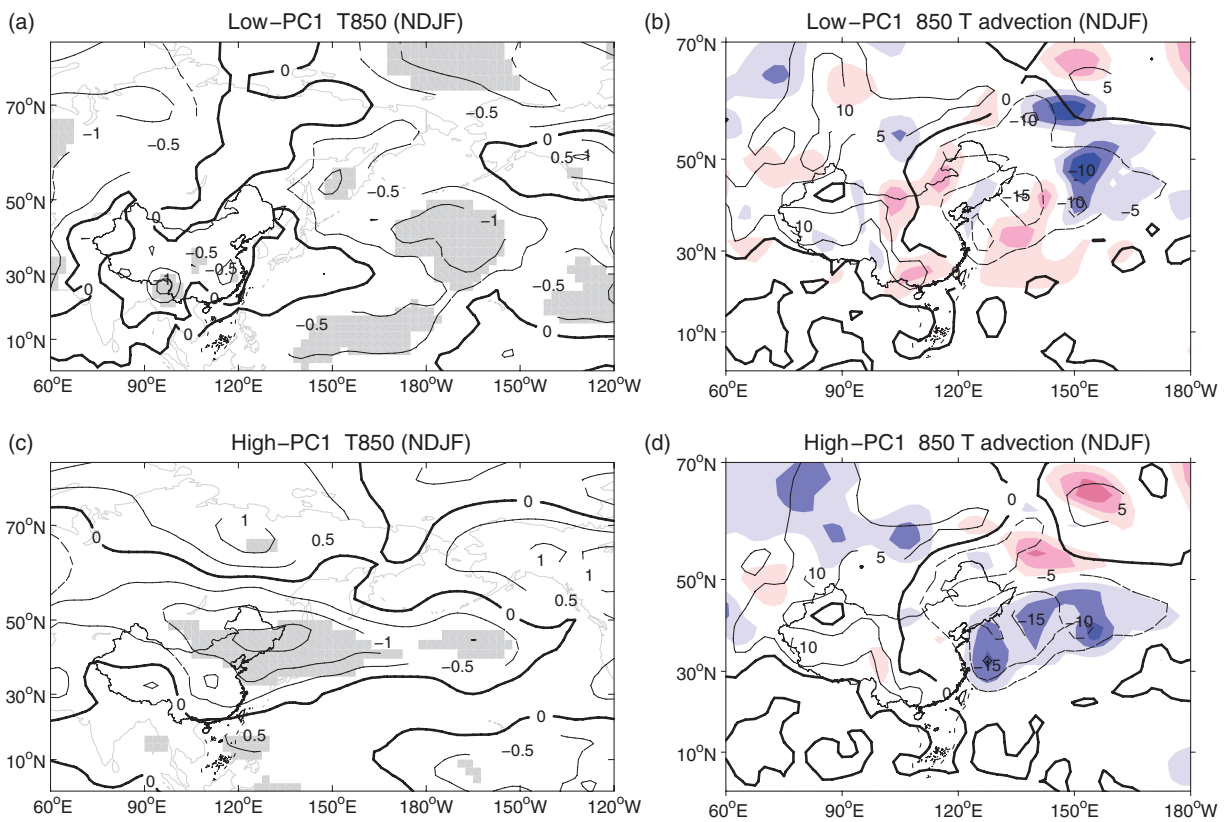


Figure 6. Composite differences of (left) 850 hPa air temperature ($CI = 0.5^{\circ}\text{C}$) between (a) the low and normal KS Qnet winters and (c) the high and normal KS Qnet winters. The shading in the left panels indicates the 95% confidence level based on Student's *t*-test. Composite contours of (right) 850 hPa temperature advection ($CI = 10^{-5} \text{ }^{\circ}\text{C s}^{-1}$) for (b) the ten low KS Qnet winters and (d) nine high KS Qnet winters. The warm (cold) colour in the right panels indicates the positive (negative) anomalies compared with the normal KS Qnet winters.

Along with the atmospheric circulation showing different patterns in the high and low winter Qnet over KS, the water vapour flux changes significantly as well, as indicated in Figure 5(b) and (d), and induces a precipitation anomaly. From the composite difference of the station-based precipitation (Figure 7(c)) between the high and low phase of the KS Qnet winters, the rainfall in the high KS Qnet winters is much less over most of China, except in the western region, and especially in South China and the Yellow-Huaihe area with respect to the low phase, which is consistent with the above difference of the water vapour flux divergence.

3.3. Lagged influence of the winter KS Qnet variation on regional climate in China

It has been documented that the SST and turbulent heat flux variations over the KS may affect the regional climate condition of the following spring or even summer (e.g. Zhang *et al.*, 2007; Zhou *et al.*, 2011; Wang *et al.*, 2012). To determine a more direct thermal variable than SST linking the ocean and atmosphere, it is well worth exploring the lagged effects of the winter KS Qnet on the climate in China to evaluate the potential predictability of climate in China in the spring based on the KS Qnet in the preceding winter.

Figure 7(b) presents the composite difference of the station-based SAT in the following spring between the

high and low KS Qnet years. Compared to the colder winters over most of northern China in the high phase of KS Qnet (See Figure 7(a)), the air temperature tends to be relatively warm in the following spring over most parts of China, especially in North China and the Yangtze-Huaihe region, with respect to the low phase of the KS Qnet. Figure 8(a) and (c) are the composite differences of air temperature and its corresponding advection at 1000 hPa between the high and low KS Qnet phase in the following spring, respectively. The results present similar intensifications of the warming at 1000 hPa in the eastern region of China, especially in the region between the Yellow River and Yangtze River, whereas the temperature is colder in the vicinity of the KS region (Figure 8(a)). This anomalous temperature dipole is caused by the opposite temperature advectations with positive anomalies over the central and eastern region of China and negative anomalies along KS in the following spring (Figure 8(c)).

Figure 7(d) shows the composite differences in station-based precipitation in the following spring between the high and low KS Qnet years. Different from the anomalous pattern of precipitation in the simultaneous winters (see Figure 7(c)), the precipitation in the low KS Qnet phase appears as a northwest-southeast band with more precipitation in the central and eastern regions of China, especially in the Yangtze-Huaihe region, compared to the high KS Qnet phase. To explore the possible reason for

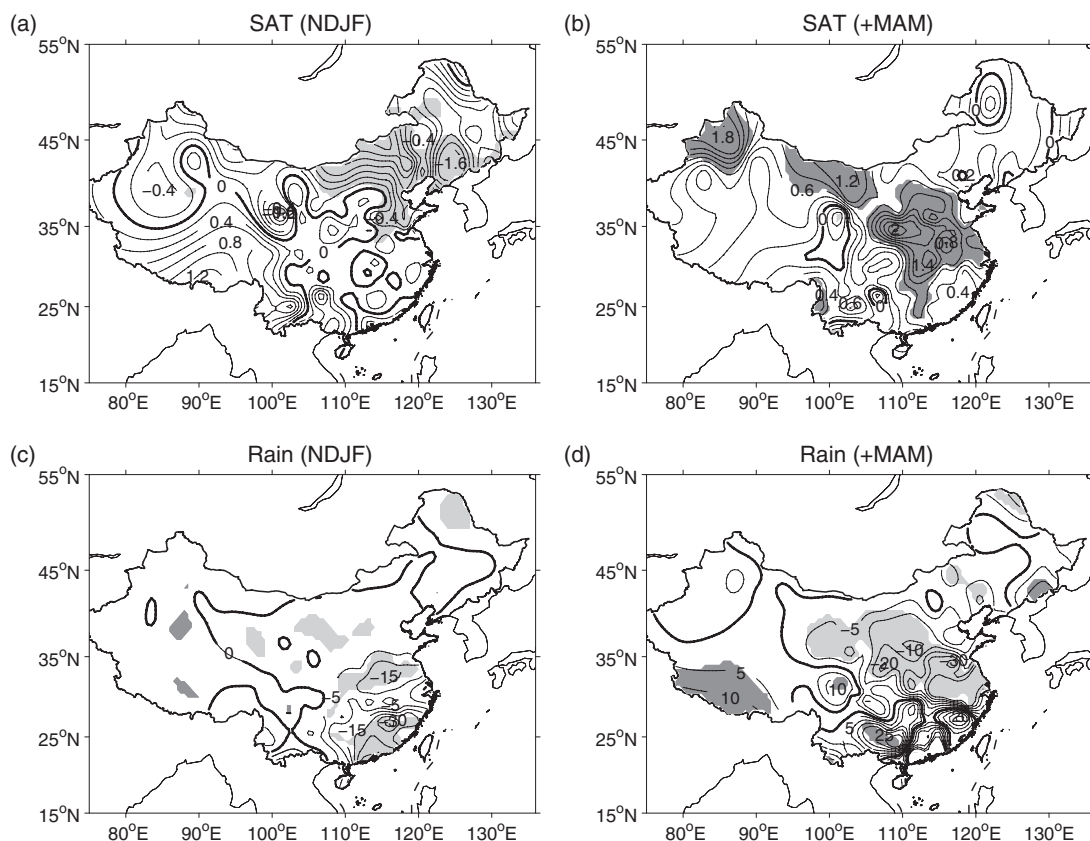


Figure 7. Composite differences of (upper) station-based SAT ($CI = 0.2^{\circ}C$) and (below) station-based precipitation ($CI = 5\text{ mm}$) (left) in simultaneous winter (NDJF) and (right) in the following spring (MAM) between the high and low KS Qnet years. The shading indicates the 95% confidence level based on Student's *t*-test.

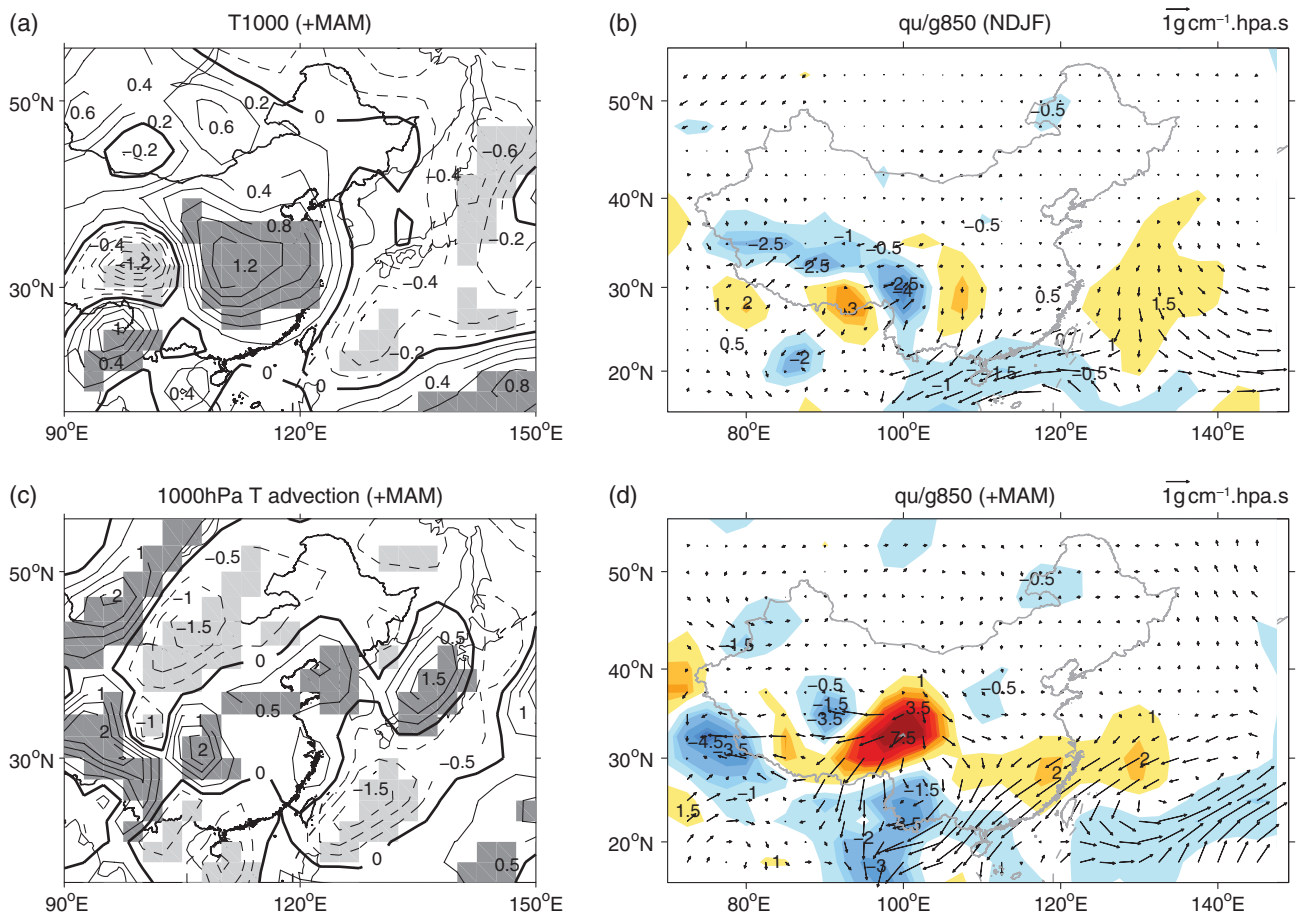


Figure 8. Composite differences of (a) 1000 hPa air temperature ($CI=0.2^{\circ}\text{C}$) and (c) its advection ($CI=0.5 \times 10^{-5}^{\circ}\text{C s}^{-1}$) in the following spring and 850 hPa vapour flux (vector, $\text{g cm}^{-1}\cdot\text{hpa}\cdot\text{s}$) and the corresponding divergence (colour shading, $10^{-8} \text{ g cm}^{-2}\cdot\text{hpa}\cdot\text{s}$) (b) in simultaneous winter and (d) in the following spring between the high and low KS Qnet years. The grey shading in the left panels indicates the 95% confidence level based on Student's *t*-test.

the above anomalous precipitation, the composite differences of the water vapour flux between the high and low KS Qnet years in the simultaneous winter (Figure 8(b)) and the following spring (Figure 8(d)) are analyzed. The prominent features are an anomalous cyclone south of the Japan Islands and anomalous northeasterly vapour flux along the northwestern flank in the following spring (Figure 8(d)), which is different from that in the previous winter. Correspondingly, the anomalous water vapour fluxes diverge over eastern China and converge over southern China, which explain well the difference of precipitation pattern between the high and low Qnet winters in the following spring. To further explore what caused the above difference, we combined the differences of the 850 hPa vapour flux between the low and normal KS Qnet winters (Figure 9(a)) and the high and normal KS Qnet winters (Figure 9(c)), respectively. Clearly, there is an anomalous anticyclone south of Taiwan Island in the low KS Qnet phase (Figure 9(a)) that enhances the southwesterly wind and transfers much more vapour to the Yangtze River basin, even reaching the Yangtze-Huaihe region. Moreover, the anomalous cold easterlies from the Sea of Japan influence northern China and join with warmer southwesterlies around the region 30°N - 40°N . Then, the

anomalous water vapour from southwesterly and easterly converges around the Yangtze region. Figure 9(b) shows the different composites of the vertical circulation associated with the meridional-mean zonal wind in the region 30°N - 40°N between the low and normal KS Qnet phase in the following spring. Obviously, the upward motion appears in the region from 110°E to 120°E , which corresponds well with more precipitation in the eastern region of China between the Yellow River and Yangtze River. Additionally, the anomalous easterlies throughout the whole troposphere appear over the KS region (125°E - 145°E). Contrary to the low KS Qnet phase, the water vapour transportation and its divergence (Figure 9(c)), and vertical atmospheric circulation (Figure 9(d)) barely change with the weak anomalous cyclone south of Japan, and the anomalous easterly winds are only in the lower troposphere and the anomalous westerlies in the upper troposphere in the high KS Qnet phase.

4. Discussion

From the composite differences of the SLP and 500 hPa geopotential height (see Figure 4) in the high KS Qnet phase, there is a noticeable northwest-southeast dipole

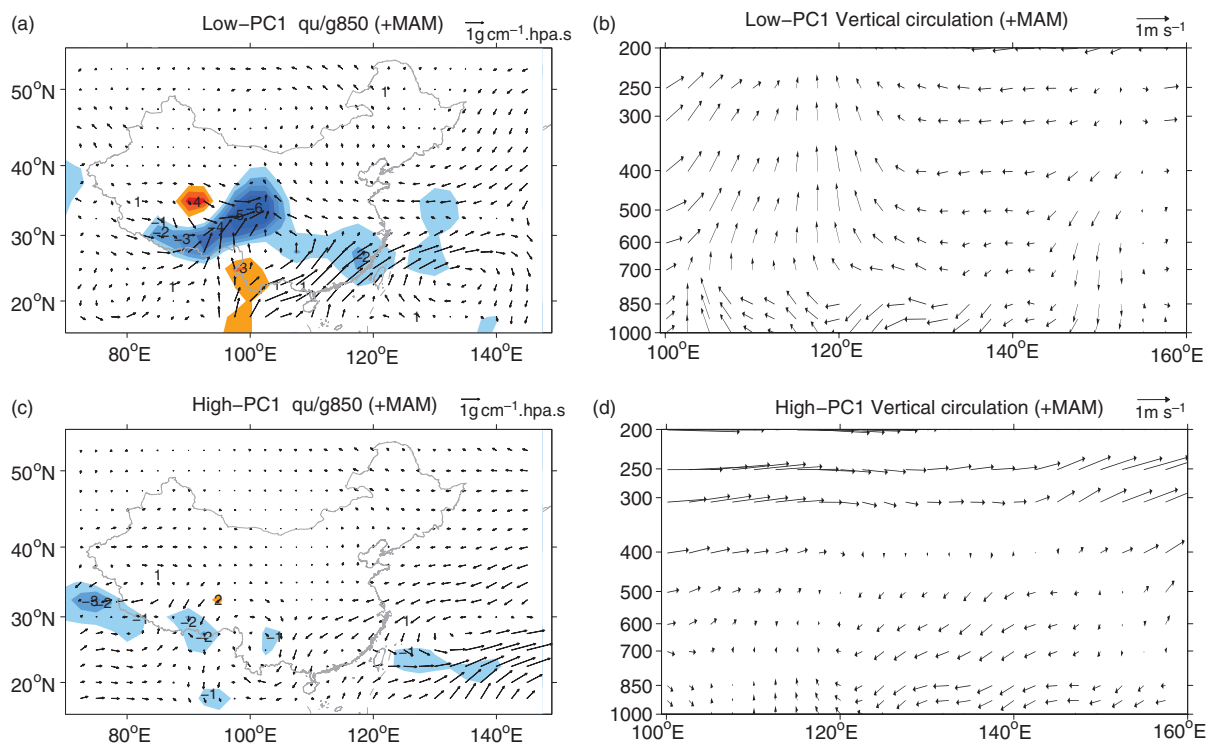


Figure 9. Composite differences of (left) 850 hPa vapour flux (vector, $\text{g cm}^{-1}\text{hPa}\cdot\text{s}$) and the corresponding divergence (colour shading, $10^{-8} \text{ g cm}^{-2}\text{hPa}\cdot\text{s}$) and (right) the vertical circulation (m s^{-1}) associated the meridional-mean zonal wind in the region 30°N – 40°N between (upper) the low and normal KS Qnet phase and (below) the high and normal KS Qnet phase in the following spring.

with a low pressure anomaly over the Aleutian region and a high pressure over Siberia, implying both an enhanced Aleutian low and Siberia high. This corresponding relation is also found in the papers of Liu and Wu (2004) and Yulaeva *et al.* (2001) with the coupled simulations. They revealed that the atmospheric circulation forced by the KS heat flux tends to be associated with low pressure in the North Pacific (warm-low response downstream) and high pressure in Siberia (cold-high response upstream). Based on the singular value decomposition (SVD) analysis of the 500 hPa geopotential height and Qnet around the KS region using the observation combined with a coupled model, Liu *et al.* (2006) also demonstrated that since the increasing of the upward Qnet over the KS region, the ocean loses more heat to warm the overlying atmosphere, and there are low pressure anomalies in the North Pacific. It is known that the East Asia winter monsoon (EAWM) is characterized by a cold Siberia high and warm Aleutian low with a strong northwesterly wind between them (Ding, 1994; Huang *et al.*, 2003, 2007, 2012; Chan and Li, 2004; Chang *et al.*, 2006; Wang *et al.*, 2009a, 2009b; Wang and Chen, 2010). Therefore, the increasing upward Qnet develops the EAWM by influencing the Siberia high upstream and the Aleutian low downstream. In turn, the enhanced EAWM further influences the Qnet over the KS mainly via the turbulent heat flux. This is because during the cold season, the local heat fluxes in the western boundary currents are strongly dependent on wind direction (Zolina and Gulev, 2003; Konda *et al.*, 2010), and the prevailing cold, dry continental airflow associated with EAWM induces

a sharp increase of heat and moisture release, which has been proven by Taguchi *et al.* (2009) using a pair of atmospheric regional model hindcast experiments. Whereas in the low KS Qnet phase, the positive pressure anomalies around the KS feature a weakened mid-tropospheric East Asia trough, which indicates weakened EAWM circulation (Huang *et al.*, 2012; Chen *et al.*, 2013). To verify the relationship of the EAWM and winter Qnet over the KS, the EAWM strength index developed by Wang *et al.* (2009a) is adopted here. We analyzed the normalized winter monthly (Nov., Dec., Jan., and Feb.) 500 hPa geopotential height over East Asia and the western North Pacific through the EOF method. Note that the sample is 104 months. The first spatial mode was found to reflect the strength of the East Asia trough (Figure 10(a)), and the corresponding normalized PC1 was defined as the EAWM strength index (Figure 10(b), the solid line) (Wang *et al.*, 2009a; Wang and Chen, 2010). Clearly, the winter mean Qnet over KS has a strong relationship with the EAWM at the interannual timescale, and their detrended correlation coefficient reaches 0.85, which is far above the 99% confidence level (Figure 10(b)). In addition, on the decadal timescale, the winter mean EAWM index also experienced a decadal weakening around the mid-1980s (Nakamura *et al.*, 2002; Wang *et al.*, 2009b), then recovered from its weak epoch and re-amplified in the mid-1990s a decadal re-amplification after the mid-1990s (Wang and Chen, 2014), which is consistent with the decadal variability of the winter Qnet for the period of 1984–2009. Moreover, the correlation coefficient of the 9-year low-pass

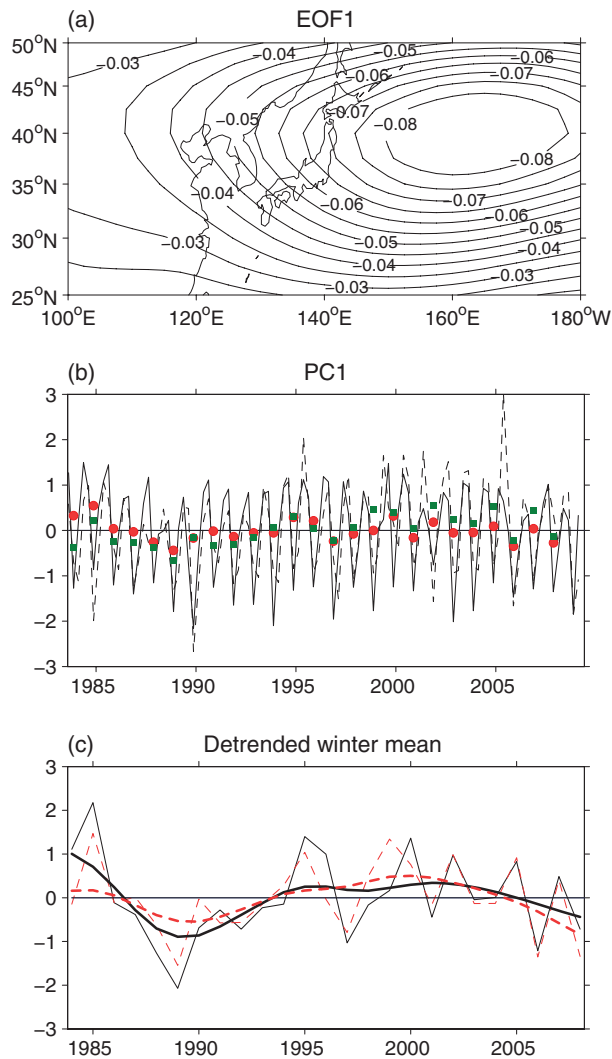


Figure 10. (a) The first EOF mode of the winter monthly (Nov., Dec., Jan., Feb.) 500 hPa geopotential height for the years 1984–2009. (b) The corresponding normalized PC time series for the first EOF mode (the solid line) shifted to the left (i.e. lag) by 1 month to obtain a maximum correlation ($r=0.72$) with the PC1 of the Qnet (the dashed line). The variance explained is 78%. Circle (square) markers represent winter mean values for the black solid (dash) line, with the detrend correlation coefficient of 0.85. (c) The detrended winter mean for the EAWM (thin solid) and Qnet (thin dashed) with the 9-year low-pass components (thick lines) using the Gaussian-type filter.

components of the detrended Qnet and EAWM indices reaches 0.80 and greater than 95% confidence level for the period 1984–2007 (Figure 10(c)). To further explore the detailed relationship of the KS Qnet and EAWM, the lead-lag correlation was examined and is shown in Figure 10(b); it indicates that during the wintertime, the Qnet intensity led by 1 month to obtain a maximum correlation ($r=0.72$) with the EAWM strength. That is, the positive Qnet anomaly over the KS forced the overlying atmospheric circulation with a deepening Aleutian low and an enhanced Siberia high and then enhanced the EAWM strength with a nearly 1-month delay. During the stronger EAWM winters, the northwesterly wind enhances and cools the near-surface air overlying the KS region,

which in turn increases the upward heat flux and cools the SST accordingly. As for the decadal timescale, the Qnet for a longer period extending to 1977 is also examined based on the dataset from the NCEP/NCAR (figure is not shown). Consistent result is found that the Qnet over the KS is not only closely associated with EAWM on interannual timescale ($r=0.82$), but also on decadal timescale ($r=0.68$). Overall, the KS Qnet variations influence the climate in China in the upstream primarily by influencing the EAWM via the anomalous low pressure response downstream (Aleutian low) and high pressure response upstream (Siberia high) in the boreal wintertime. Furthermore, this mechanism is able to reasonably explain the climate variation in China as well. In the high phase of the KS Qnet winters, most of northern China, especially Northeast China, is dominated by the stronger cold temperature advection caused by the enhanced EAWM in the simultaneous winter (Figure 6(d)). Air temperature at 850 hPa (Figure 6(c)), station-based SAT (Figure 7(a)) and SAT from the Climatic Research Unit (CRU) (figure is not shown) confirm the colder winters in the high phase of KS Qnet years. Moreover, the enhanced northwesterly wind governs the whole Chinese mainland for the stronger EAWM winters and forces the southeasterly wind back to the ocean (see Figure 5(d)), thereby reducing the precipitation in the east and south regions of China (see Figure 7(d)).

An anomalously high Qnet over the KS implies more heat loss from the ocean to the overlying atmosphere and then dampens the local SST anomaly directly (Frankignoul and Kestenare, 2002; Frankignoul *et al.*, 2004). The increasing Qnet is always accompanied by the deepened Aleutian low (Yulaeva *et al.*, 2001; Liu and Wu, 2004; Liu *et al.*, 2006), which drives larger amounts of cold water from high latitudes along its western flank and cools the SSTs over the KS as well. This Qnet–SST negative feedback partially controls the persistence and amplitude of the SST anomalies, which causes the Qnet not to vanish but to decay in the following spring to influence the atmospheric circulation. Therefore, in the following springtime, the Qnet for the high (low) phase still shows an anomalously positive (negative) pattern, but the intensity is weaker (figure is not shown). In springtime when the transition from EAWM to East Asian summer monsoon (EASM) occurs, the northwesterly wind retreats northward and only controls the region over Northeast China, the southwesterly wind enhances and influences the region south of the Yangtze River, and the Huang–Yangtze plain between them is dominated by a weak anti-cyclone (figure is not shown). If the Qnet is smaller in the preceding winter, then southern China is controlled by anomalously strong warm southwesterlies because of the anomalous anticyclone south of the Taiwan Island, whereas northern China is influenced by the anomalous cold and wet easterlies from the Sea of Japan in the subsequent spring. Therefore, northern China, especially north of the Yangtze River, appears to have a prominent anomalous cold advection and is colder than normal. In addition, the stronger warm and wet southwesterly wind joins with the anomalously cold

easterlies from the Sea of Japan over the Yellow-Yangtze region (30°N–40°N, 100°E–120°E), accompanied by the obviously anomalous upward motions, which favours more rainfall in these regions.

5. Conclusion

In this study, the variation of the Qnet over the KS in boreal winter from 1984 to 2009 and its impact on the climate in China are investigated. Results show that the KS Qnet undergoes a steady enhancement in the period 1984–2009. In addition, KS Qnet is characterized by obvious interannual variability with quasi-5 year oscillation cycle, as well as decadal variability shifting from positive to negative around the mid-1980s, then recovered from its weak epoch and re-amplified in the mid-1990s.

The winter Qnet variations over the KS play different roles on the climate in China by impacting the atmospheric circulation in the simultaneous winter and the following spring. During the wintertime when East Asia is under the control of strong northwesterly winds, the KS Qnet variation impacts the climate in China mainly via EAWM by motivating a low pressure response downstream and a high pressure response upstream. The high Qnet over the KS is always accompanied with enhanced EAWM which indicates colder winters in Northeast China, while in the low Qnet winters, the weakened EAWM with the enhanced anti-cyclone over the South China Sea induces more rain over southern China. In the following spring, the persistent but weaker Qnet anomaly over KS primarily impacts the climate in the central and eastern region of China, which happens to be located west of the KS. For example, if the Qnet over the KS is in the low phase, the following spring tends to colder and wetter than normal. Therefore, this study deepens the insights into the relationship between the KS Qnet and climate in China to a certain extent and will be helpful in improving regional climate predictions in China in the springtime.

Acknowledgements

This work is supported by the National Basic Research Program of China (2013CB956201 and 2010CB950401), the National Natural Science Foundation of China (Grant No. 40976011) and China 111 project (No. B 13045), and YPG is supported in part by JIFRESSE, UCLA, USA.

References

Bengtsson L, Hodges KI, Roeckner E. 2006. Storm tracks and climate change. *J. Clim.* **19**: 3518–3543, DOI: 10.1175/JCLI3815.1.
 Bond NA, Cronin MF. 2008. Regional weather patterns during anomalous air-sea fluxes at the Kuroshio Extension Observatory (KEO). *J. Clim.* **21**: 1680–1697.
 Booth BBB, Dunstone NJ, Halloran PR, Andrews T, Bellouin N. 2012. Aerosols implicated as a prime driver of twentieth-century North Atlantic climate variability. *Nature* **484**: 228–232.
 Cayan DR. 1992. Latent and sensible heat flux anomalies over the northern oceans: driving the sea surface temperature. *J. Phys. Oceanogr.* **22**: 859–881.

Chan JCL, Li CY. 2004. The East Asia winter monsoon. In *East Asian Monsoon*, Chang CP (ed). World Scientific Publishing Co Pet Ltd.: Singapore, 54–106.
 Chang EKM, Lee S, Swanson KL. 2002. Storm track dynamics. *J. Clim.* **15**: 2163–2183.
 Chang CP, Wang Z, Hendon H. 2006. The Asian winter monsoon. In *The Asian Monsoon*, Wang B (ed). Praxis: Berlin, 89–127.
 Chen W, Wei K, Wang L, Zhou Q. 2013. Climate variability and mechanisms of the East Asian winter monsoon and the impact from the stratosphere. *Chin. J. Atmos. Sci.* **37**: 425–438.
 Ding YH. 1994. *Monsoons over China*. Kluwer Academic Publishers: Dordrecht, The Netherlands.
 Frankignoul C, Kestenare E. 2002. The surface heat flux feedback. Part I: estimates from observations in the Atlantic and the North Pacific. *Clim. Dyn.* **19**: 633–647.
 Frankignoul C, Kestenare E, Botzet M, Carril AF, Drange H, Pardaens A, Terray L, Sutton R. 2004. An intercomparison between the surface heat flux feedback in five coupled models, COADS and the NCEP reanalysis. *Clim. Dyn.* **22**: 373–388.
 Gulev SK, Latif M, Keenlyside N, Park W, Koltermann KP. 2013. North Atlantic Ocean control on surface heat flux on multidecadal timescales. *Nature* **499**: 464–467.
 Hoskins BJ, Hodges KI. 2002. New perspectives on the Northern Hemisphere winter storm tracks. *J. Atmos. Sci.* **59**: 1041–1061.
 Hoskins BJ, Valdes PJ. 1990. On the existence of storm-tracks. *J. Atmos. Sci.* **47**: 1854–1864.
 Huang J, Higuchi K, Shabbar A. 1998. The relationship between the North Atlantic Oscillation and El Niño-Southern Oscillation. *Geophys. Res. Lett.* **25**: 2707–2710.
 Huang RH, Zhou LT, Chen W. 2003. The progresses of recent studies on the variabilities of the East Asian monsoon and their causes. *Adv. Atmos. Sci.* **20**: 55–69.
 Huang RH, Chen JL, Huang G. 2007. Characteristics and variations of the East Asian monsoon system and its impacts on climate disasters in China. *Adv. Atmos. Sci.* **24**: 993–1023.
 Huang RH, Chen JL, Wang L, Lin ZD. 2012. Characteristics, processes and causes of the spatio-temporal variabilities of the East Asian monsoon system. *Adv. Atmos. Sci.* **29**: 910–942.
 Joyce TM, Kwon YO, Yu L. 2009. On the relationship between synoptic wintertime atmospheric variability and path shifts in the Gulf Stream and the Kuroshio extension. *J. Clim.* **22**: 3177–3192, DOI: 10.1175/2008JCLI2690.1.
 Kalnay E, Kanamitsu M, Kistler R, Collins W, Deaven D, Gandin L, Iredell M, Saha S, White G, Woollen J, Zhu Y, Leetmaa A, Reynolds R, Chelliah M, Ebisuzaki W, Higgins W, Janowiak J, Mo KC, Ropelewski C, Wang J, Jenne R, Joseph D. 1996. The NCEP/NCAR 40-year reanalysis project. *Bull. Am. Meteorol. Soc.* **77**: 437–470.
 Kelly KA, Small RJ, Samelson RM, Qiu B, Joyce TM, Kwon YO, Cronin M. 2010. Western boundary currents and frontal air-sea interaction: Gulf Stream and Kuroshio extension. *J. Clim.* **23**: 5644–5667.
 Konda M, Ichikawa H, Tomita H, Cronin MF. 2010. Surface heat flux variations across the Kuroshio extension as observed by surface flux buoys. *J. Clim.* **23**: 5206–5221.
 Kubota M, Iwasaka N, Kizu S, Konda M, Kutsuwada K. 2002. Japanese ocean flux data sets with use of remote sensing observations (J-OFURO). *J. Oceanogr.* **58**: 213–225.
 Kwon YO, Alexander MA, Nicholas AB, Frankignoul C, Nakamura H, Qiu B, Thompson LA. 2010. Role of Gulf Stream, Kuroshio-Oyashio and their extensions in large-scale atmosphere-ocean interaction: a review. *J. Clim.* **23**: 3249–3281, DOI: 10.1175/2010JCLI3343.1.
 Li YF, Ding YH. 2002. Sea surface temperature, land surface temperature and the summer rainfall anomalies over eastern China (in Chinese). *Clim. Environ. Res.* **7**: 88–101.
 Li G, Ren BH, Yang CY, Zheng JQ. 2011. Net air-sea surface heat flux during 1984–2004 over the North Pacific and North Atlantic oceans (10°–50°): annual mean climatology and trend. *Theor. Appl. Climatol.* **104**: 387–401, DOI: 10.1007/s00704-010-0351-2.
 Liu ZY, Wu LX. 2004. Atmospheric response to North Pacific SST: the role of ocean-atmosphere coupling. *J. Clim.* **17**: 1859–1882.
 Liu QY, Wen N, Yu YQ. 2006. The role of the Kuroshio in the winter North Pacific ocean-atmospheric interaction: comparison of a coupled model and observations. *Adv. Atmos. Sci.* **23**: 181–189.
 Minobe S, Kuwano-Yoshida A, Komori N, Xie S, Small R. 2008. Influence of the Gulf Stream on the troposphere. *Nature* **452**: 206–209, DOI: 10.1038/nature06690.
 Nakamura H, Izumi T, Sampe T. 2002. Interannual and decadal modulations recently observed in the Pacific storm track activity and East Asian winter monsoon. *J. Clim.* **15**: 1855–1874.

- Nakamura H, Sampe T, Tanimoto Y, Shimpo A. 2004. Observed associations among storm tracks, jet streams and midlatitude oceanic fronts. *Geophys. Monogr. Ser.* **147**: 329–345, DOI: 10.1029/147GM18.
- Ni DH, Sun ZB, Chen HS, Zhu WJ. 2004. Spatial/temporal features of summer SSTA in the Kuroshio current region and its relation to summer precipitation in China (in Chinese). *J. Nanjing Inst. Meteorol.* **27**: 310–316.
- Ninomiya K. 2006. Features of the polar air outbreak and the energy balance in the transformed air-mass observed over the Japan Sea. *J. Meteorol. Soc. Jpn.* **84**: 529–542.
- North GR, Moeng FJ, Bell TL, Cahalan RF. 1982a. The latitude dependence of the variance of zonally averaged quantities. *Mon. Weather Rev.* **110**: 319–326.
- North GR, Bell TL, Cahalan RF, Moeng FJ. 1982b. Sampling errors in the estimation of empirical orthogonal functions. *Mon. Weather Rev.* **110**: 699–706.
- Qiu B. 2000. Interannual variability of the Kuroshio extension and its impact on the wintertime SST field. *J. Phys. Oceanogr.* **30**: 1486–1502.
- Taguchi B, Nakamura H, Nonaka M, Xie SP. 2009. Influences of the Kuroshio/Oyashio extensions on air–sea heat exchanges and storm-track activity as revealed in regional atmospheric model simulations for the 2003/04 cold season. *J. Clim.* **22**: 6536–6560.
- Tokinaga H, Tanimoto Y, Nonaka M, Taguchi B, Fukamachi T, Xie SP, Nakamura H, Watanabe T, Yasuda I. 2006. Atmospheric sounding over the winter Kuroshio extension: effects of surface stability on atmospheric boundary layer structure. *Geophys. Res. Lett.* **33**: L04703, DOI: 10.1029/2005GL025102.
- Tokinaga H, Tanimoto Y, Xie SP, Sampe T, Tomita H, Ichikawa H. 2009. Ocean frontal effects of the vertical development of clouds over the western North Pacific: in situ and satellite observations. *J. Clim.* **22**: 4241–4260.
- Tomita T, Sato H, Nonaka M, Hara M. 2007. Interdecadal variability of the early summer surface heat flux in the Kuroshio region and its impact on the Baiu frontal activity. *Geophys. Res. Lett.* **34**: L10708, DOI: 10.1029/2007GL029676.
- Vautard R, Yiou P, Ghil M. 1992. Singular-spectrum analysis: a toolkit for short, noisy chaotic signals. *Phys. Nonlinear Phenom.* **58**: 95–126.
- Wallace JM, Gutzler DS. 1981. Teleconnections in the geopotential height field during the Northern Hemisphere winter. *Mon. Weather Rev.* **109**: 784–812.
- Wallace J, Hobbs PV. 2006. *Atmospheric Science: An Introductory Survey*, 2nd edn. Academic Press: New York, NY, 483.
- Wang L, Chen W. 2010. How well do existing indices measure the strength of the East Asian winter monsoon? *Adv. Atmos. Sci.* **27**: 855–870.
- Wang L, Chen W. 2014. The East Asian winter monsoon: re-amplification in the mid-2000s. *Chin. Sci. Bull.* **59**: 430–436.
- Wang L, Feng J. 2011. Two major modes of the wintertime precipitation over China. *Chin. J. Atmos. Sci.* **35**: 1105–1116.
- Wang SW, Zhao ZC, Chen ZH, Wei SL, Yu PS. 1980. The Interactions between the sea surface temperature and the atmospheric circulation in the winter half year (in Chinese). *Acta Oceanol. Sin.* **2**: 27–39.
- Wang L, Chen W, Zhou W, Huang R. 2009a. Interannual variations of East Asian trough axis at 500 hPa and its association with the East Asian winter monsoon pathway. *J. Clim.* **22**: 600–614.
- Wang L, Huang RH, Gu L, Chen W, Kang LH. 2009b. Interdecadal variations of the East Asian winter monsoon and their association with quasi-stationary planetary wave activity. *J. Clim.* **22**: 4860–4872.
- Wang SS, Guan YP, Li ZJ, Chao Y, Huang JP. 2012. Preliminary analyses on characteristics of sea surface temperatures in Kuroshio and its extension and relations to atmospheric circulations. *Acta Phys. Sin.* **61**: 169201.
- Weng XC, Zhang QL, Yang YL, Yan YZ. 1996. The Kuroshio heat transport in the East China Sea and its relation to the precipitation in the rainy season in the Huanghuai Plain area (in Chinese). *Oceanol. Limnol. Sin.* **27**: 237–245.
- Wu L, Lee DE, Liu Z. 2005. The 1976/77 North Pacific climate regime shift: the role of subtropical ocean adjustment and coupled ocean–atmosphere feedbacks. *J. Clim.* **18**: 5125–5140.
- Xue H, Bane JJM, Goodman LM. 1995. Modification of the Gulf Stream through strong air–sea interactions in winter: observations and numerical simulations. *J. Phys. Oceanogr.* **25**: 533–557.
- Yu L, Weller RA. 2007. Objectively analyzed air–sea heat fluxes (OAFlux) for the global oceans. *Bull. Am. Meteorol. Soc.* **88**: 527–539.
- Yu L, Jin X, Weller RA. 2007. Annual, seasonal, and interannual variability of air–sea heat fluxes in the Indian Ocean. *J. Clim.* **20**: 3190–3209.
- Yu L, Jin X, Weller RA. 2008. Multidecade global flux datasets from the objectively analyzed air–sea fluxes (OAFlux) project: latent and sensible heat fluxes, ocean evaporation, and related surface meteorological variables. OAFlux Project Technical Report, Woods Hole Oceanographic Institution, Woods Hole, MA.
- Yulaeva E, Schneider N, Pierce DW, Barnett TP. 2001. Modeling of North Pacific climate variability forced by oceanic heat flux anomalies. *J. Clim.* **14**: 4027–4046.
- Zhang QL, Weng XC, Cheng MH. 1999. Relationship between the precipitation in the rainy season in North China and the tropical western Pacific warm pool (in Chinese). *Plateau Meteorol.* **4**: 575–583.
- Zhang YC, Rossow WB, Lacis AA, Oinas V, Mishchenko MI. 2004. Calculation of radiative fluxes from the surface to top of atmosphere based on ISCCP and other global data sets: refinements of the radiative transfer model and the input data. *J. Geophys. Res.* **109**: D19105, DOI: 10.1029/2003JD004457.
- Zhang TY, Sun ZB, Li ZX, Wang DY. 2007. Relation between spring Kuroshio SSTA and summer rainfall in China. *J. Trop. Meteorol.* **23**: 189–195.
- Zhang YC, Zhang LF, Luo Y. 2010. The coupled mode between the Kuroshio region marine heating anomaly and the north pacific atmospheric circulation in wintertime. *J. Trop. Meteorol.* **16**: 51–58.
- Zhao FM, Zhu XJ, Li F, Wang ZQ, Gu JY, Wang ML. 2007. Relationship between SSTA in Japan current region and temperature and precipitation in China winter (in Chinese). *Meteorol. Environ. Sci.* **30**: 28–31.
- Zhou LY, Xu HM, Xu MM, Zhu SX. 2011. The variability characteristics of turbulent heat fluxes in winter over the East China Sea and the relation between rainfall and temperature in China (in Chinese). *J. Meteorol. Sci.* **31**: 558–566.
- Zolina O, Gulev SK. 2003. Synoptic variability of ocean–atmosphere turbulent fluxes associated with atmospheric cyclones. *J. Clim.* **16**: 3023–3041.